



HAL
open science

Intensity noise in difference frequency generation-based tunable femtosecond MIR sources

Q Bournet, M Natile, M Jonusas, F Guichard, Y Zaouter, M Joffre, A Bonvalet, F Druon, Marc Hanna, P Georges

► **To cite this version:**

Q Bournet, M Natile, M Jonusas, F Guichard, Y Zaouter, et al.. Intensity noise in difference frequency generation-based tunable femtosecond MIR sources. *Optics Express*, 2023, 31 (8), pp.12693-12702. 10.1364/oe.486509 . hal-04072416

HAL Id: hal-04072416

<https://hal-iogs.archives-ouvertes.fr/hal-04072416>

Submitted on 18 Apr 2023

HAL is a multi-disciplinary open access archive for the deposit and dissemination of scientific research documents, whether they are published or not. The documents may come from teaching and research institutions in France or abroad, or from public or private research centers.

L'archive ouverte pluridisciplinaire **HAL**, est destinée au dépôt et à la diffusion de documents scientifiques de niveau recherche, publiés ou non, émanant des établissements d'enseignement et de recherche français ou étrangers, des laboratoires publics ou privés.



Intensity noise in difference frequency generation-based tunable femtosecond MIR sources

Q. BOURNET,^{1,2,*} M. NATILE,² M. JONUSAS,³ F. GUICHARD,²
Y. ZAOUTER,² M. JOFFRE,³  A. BONVALET,³  F. DRUON,¹ 
M. HANNA,¹  AND P. GEORGES¹ 

¹Université Paris-Saclay, Institut d'Optique Graduate School, CNRS, Laboratoire Charles Fabry, 91127 Palaiseau, France

²Amplitude, 11 Avenue de Canteranne, Cité de la Photonique, 33600 Pessac, France

³Laboratoire d'Optique et Biosciences, Ecole Polytechnique, CNRS, INSERM, Institut Polytechnique de Paris, 91128 Palaiseau, France

*quentin.bournet@institutoptique.fr

Abstract: We characterize the intensity noise of two mid-infrared (MIR) ultrafast tunable (3.5–11 μm) sources based on difference frequency generation (DFG). While both sources are pumped by a high repetition rate Yb-doped amplifier delivering 200 μJ 300 fs at a central wavelength of 1030 nm, the first is based on intrapulse DFG (intraDFG), and the second on DFG at the output of an optical parametric amplifier (OPA). The noise properties are assessed through measurement of the relative intensity noise (RIN) power spectral density and pulse-to-pulse stability. The noise transfer mechanisms from the pump to the MIR beam is empirically demonstrated. As an example, improving the pump laser noise performance allows reduction of the integrated RIN (IRIN) of one of the MIR source from 2.7% RMS down to 0.4% RMS. The intensity noise is also measured at various stages and in several wavelength ranges in both laser system architectures, allowing us to identify the physical origin of their variation. This study presents numerical values for the pulse to pulse stability, and analyze the frequency content of the RINs of particular importance for the design of low-noise high repetition rate tunable MIR sources and future high performance time-resolved molecular spectroscopy experiments.

© 2023 Optica Publishing Group under the terms of the [Optica Open Access Publishing Agreement](#)

1. Introduction

Femtosecond laser sources emitting in the mid-infrared (MIR) are required for a wide range of spectroscopy applications [1,2], including life sciences. The spectral range between 3 and 15 μm , often referred to as the fingerprint region, is particularly interesting because many molecules exhibit absorption bands in this zone. Optimizing the signal to noise ratio (SNR) is essential to achieve high resolution spectroscopy [3,4], and the recent availability of high repetition rate sources (>100 kHz) has allowed to increase SNR by averaging over several laser shots, while retaining fast measurement times [5]. However, the source noise properties are a key factor to determine the achievable performance of any spectroscopic system.

One of the most used techniques to access this spectral region is difference frequency generation (DFG) [6], because of the lack of laser materials in the MIR [7], and because high power pump lasers in the near infrared (NIR) are widely available. Moreover, DFG-based sources provide broadband and tunable emission, making them highly suitable for ultrafast spectroscopy [8]. These sources can be broadly categorized into inter-pulse DFG and intra-pulse DFG (intraDFG). In the first case, pump and signal originate from two distinct pulses that do not share the same spectrum. Usually, delay lines are used to synchronize the interacting pulses. Very often, the interaction is carried out by combining the NIR pump pulse with either a white-light generation

(WLG) pulse or a WLG-seeded optical parametric amplification (OPA) signal. Broadband and tunable MIR pulses with energy conversion efficiencies between 0.2 and 2.6 % centered at 8 μm have been reported [9–11]. In intraDFG, the interacting pump and signal are two spectral parts of the same pulse. No delay lines are required in this case, simplifying the implementation and removing the possibility of delay drifts. Very broadband NIR pump sources are used for intraDFG to obtain broadband, tunable MIR sources in a simple and compact setup. The efficiency of the process is generally lower (<0.5 %, typically 0.1 % at 6–10 μm) compared to inter-pulse DFG schemes [12,13].

Although intensity noise of the laser source plays a key role in the optimization of SNR in ultrafast spectroscopy, there is a very limited number of reports of complete intensity noise characterization for the above-described MIR sources. The lack of high responsivity detectors sensitive to wavelengths above 2 μm makes noise characterization not trivial or impossible when the pulse energy is too low [14]. Huber et al. [15] characterize the noise of an intraDFG source at 10 μm and improve it using a novel active stabilization setup. Other works have characterized DFG approaches at a specific MIR wavelength [16] and with different seeders impact [17]. A systematic analysis of the noise properties of DFG sources, including e.g. the noise properties as a function of central wavelength in tunable setups, is still missing.

In this work, we focus on the intensity noise properties of MIR sources tunable between 3.5 and 11 μm based on DFG. Two different sources are analyzed, respectively based on the intraDFG and inter-pulse DFG approaches. They are both pumped by an Yb-doped ultrafast laser system at 1 μm . First, we study the pump to MIR noise transfer at a central wavelength of 8 μm for both sources. In particular, a noise reduction from 2.7% RMS down to 0.4% RMS on the intraDFG source is demonstrated by improving the NIR pump source noise performances. Second, we measure the noise characteristics as a function of central wavelength, over a tunability range exceeding an octave for both sources. The intraDFG source exhibits more wavelength-dependent noise levels, and an overall higher noise than the DFG source. This study should reveal useful for the design of future high repetition rate MIR sources for ultrafast molecular spectroscopy.

2. Experimental setup

2.1. MIR sources

IntraDFG and DFG-based experimental setups are depicted in Fig. 1(a) and (b) respectively. The first architecture is similar to the one presented in [18]. Initial driving pulses are generated by a high-energy Yb-doped-fiber amplifier (source 1 in Fig. 1(a)) (200 μJ , 260 fs, 1030 nm, 250 kHz) and spectrally broadened by a 61% efficient dual-stage nonlinear compression scheme composed of a multipass cell and a gas-filled capillary [19]. After compression using chirped mirrors, a pulse duration of 7.4 fs is measured. At the output, half of the energy is used to drive the intraDFG process in a 1-mm thick LGS crystal with an estimated intensity of $\sim 120 \text{ GW/cm}^2$. As described in [18], a bichromatic waveplate is added to optimize the intraDFG process. To maximize the process efficiency, the input chirp is finely adjusted by the insertion of a calcium fluoride (CaF_2) plate. The CaF_2 plate thickness is changed as the MIR wavelength is tuned to obtain maximum intraDFG efficiency.

For the DFG-based setup, a similar Yb-doped-fiber amplifier, operating at 100 kHz (source 2 in Fig. 1(b)), is used. The 200 μJ are split into two pathways. 140 μJ are used to pump the DFG process. 60 μJ are used to obtain the signal for the DFG via a WLG-seeded OPA. 2 μJ are used for WLG in a 15 mm-long YAG crystal. The remaining 58 μJ are frequency doubled in a BBO crystal to produce 30 μJ pulses at 515 nm. The signal from the WLG and the pump at 515 nm are temporally synchronized and spatially overlapped in a 2.5 mm-thick BBO to generate pulses over the spectral range [1150 nm; 1450 nm] with energies higher than 1 μJ . The DFG process is realized in a 2 mm-thick LGS crystal with an estimated pump intensity of $\sim 100 \text{ GW/cm}^2$. At

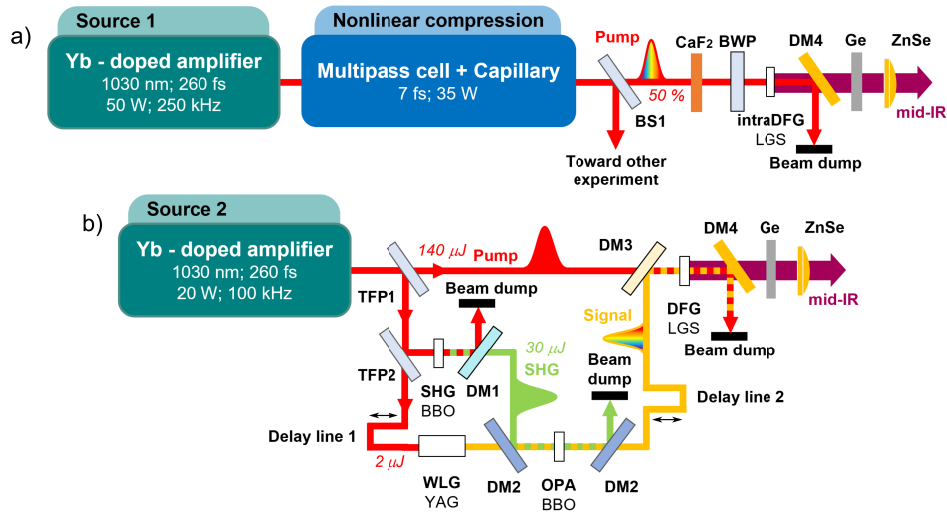


Fig. 1. Schematic of the a) intraDFG and b) DFG-based experimental setups. BS1: beam splitter 50/50; BWP: bichromatic waveplate; DM4: dichroic mirror ($R\text{-}\lambda < 2\mu\text{m}$, $T\text{-}\lambda > 2\mu\text{m}$); TFP: thin film polarizer; DM1: dichroic mirror ($R\text{-}\lambda = 1030\text{nm}$, $T\text{-}\lambda = 515\text{nm}$); DM2: dichroic mirror ($R\text{-}\lambda < 1100\text{nm}$, $T\text{-}\lambda > 1100\text{nm}$); DM3: dichroic mirror ($R\text{-}\lambda > 1100\text{nm}$, $T\text{-}\lambda = 1030\text{nm}$)

the output of both DFG and intraDFG sources a dichroic mirror (DM4) and a germanium plate (Ge) are used to filter the MIR pulses.

Figure 2(a) shows the spectral tunability measured with a home-built Fourier transform infrared (FTIR) spectrometer for both setups. They generate pulses with broadband spectra on a wide tunability range, extending from 3.5 to 11 μm .

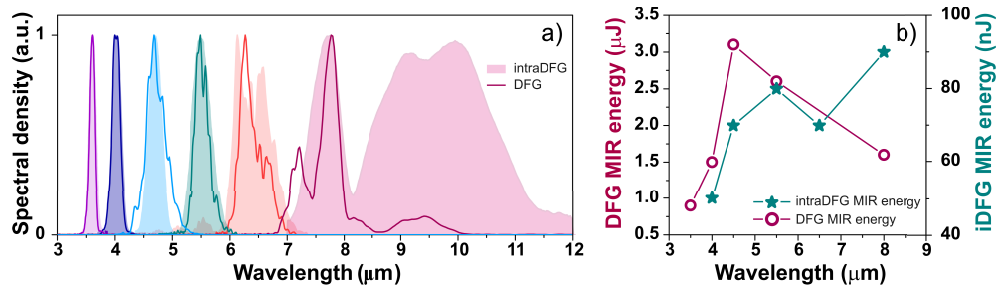


Fig. 2. (a) Measured MIR spectra for the intraDFG architecture (filled) and DFG (solid line) setups with 1- and 2-mm thick LGS crystals, respectively. (b) Corresponding pulse energies for the intraDFG (green stars) and DFG (red circles) setups.

Spectra are narrower as the central wavelength decreases because of the phase-matching properties of LGS [20]. The corresponding Fourier-transform limited (FTL) durations decrease from 131 fs to 56 fs as the central wavelength increases from 3.5 to 11 μm for the intraDFG source. For the DFG source, the FTL durations decrease from 156 fs to 74 fs. The intraDFG crystal is twice as short as the one used in the DFG experiment, thus limiting the phase-matched bandwidth in the latter case. In Fig. 2(b), the corresponding MIR pulse energies are reported for both sources. For intraDFG, energies vary from 20 to 90 nJ, corresponding to a global optical efficiency (ratio between output MIR pulse energy and incident pump energy) of 0.17% at 8

μm . For the DFG source, energies extend from $0.9 \mu\text{J}$ to $1.7 \mu\text{J}$, with a maximum of $3.1 \mu\text{J}$ at $5 \mu\text{m}$, corresponding to an optical efficiency of 1.6% at $5 \mu\text{m}$ and 0.8% at $8 \mu\text{m}$. The efficiency difference is due to a smaller number of interacting pump photons in intraDFG because the spectral density of the ultrashort NIR driving pulse is distributed over a larger bandwidth and two linear polarization states. This can be alleviated by adding a further OPA stage to the intraDFG setup, e. g. by recycling signal photons in an all in-line configuration [21].

2.2. Noise measurement setup

We now introduce the experimental setups used for intensity noise measurements. They are based on several photodiodes that are used for the various wavelength ranges, with different noise and responsivity characteristics. For the NIR wavelength range [700 nm; 1100 nm] we use a silicon-based photodiode (DET36A2/M, Thorlabs), for the wavelength range [1200 nm; 1500 nm] we use an InGaAs-based photodiode (DET10C, Thorlabs), and for the wavelength range [3 μm ; 10 μm] we use a liquid-nitrogen-cooled mercury cadmium telluride (MCT) detector (J15D16-M200-S100U-30, Teledyne Judson). The saturation level and linearity range are experimentally determined for each photodetector to define the proper optical power to be used. To limit beam pointing fluctuations to intensity noise coupling, the beam is focused onto the photodetectors using a lens. In all cases, photodetectors were covered to minimize the influence of stray light.

Two types of noise measurement are performed, denoted as pulse-to-pulse stability and relative intensity noise (RIN). The pulse-to-pulse stability is measured by sending the photodetected signal directly to a sampling oscilloscope, and using the maximum detection feature of the oscilloscope over 1000 waveforms. The pulse-to-pulse stability is the standard deviation of these maxima. This procedure is repeated 5 times and averaged for better accuracy.

The RIN measurement setups are shown in Fig. 3(a) and Fig. 3(b) for the NIR and MIR ranges respectively. They differ due to the various photodetector parameters, to optimize the measurement noise floor.

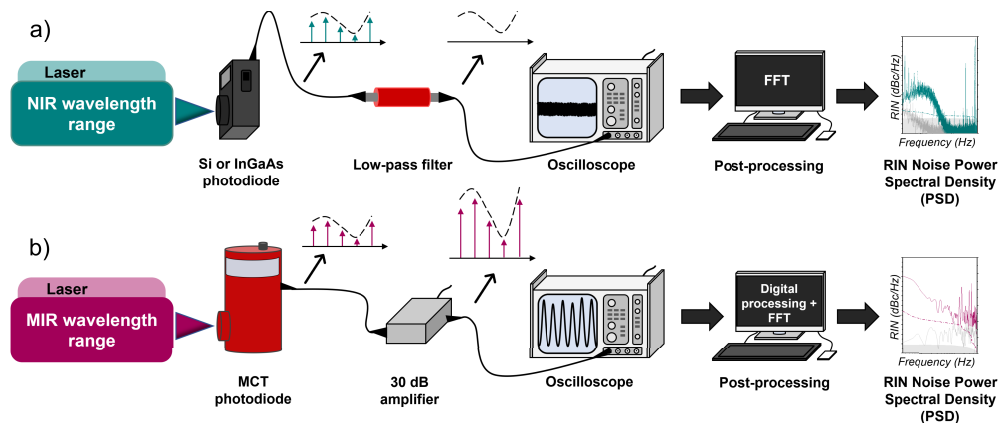


Fig. 3. (a) RIN measurement setup for the NIR wavelength range (b) RIN measurement setup for the MIR wavelength range.

To measure the RIN in the NIR wavelength range, the photodiode signal filtered by a low-pass filter is sent to a sampling oscilloscope. We choose a filter with a cutoff frequency of 50 kHz (EF124, Thorlabs), equal (DFG) or slightly lower (intraDFG) than the Nyquist frequency corresponding to the laser repetition rate. The RIN power spectral density (PSD) is obtained by Fourier transforming this signal normalized by its average value. The corresponding integrated RIN (IRIN) values are calculated by integrating the PSD from the highest frequency to the

lowest, followed by a square root operation. For all IRIN values, the measurement noise is subtracted assuming no correlation with optical noise. For the RIN in the MIR wavelength range, we measure the photodetected pulse train unfiltered, and using the full sampling rate of the oscilloscope (2.5 GSa/s) over a time window limited to 4 ms. This allows to resolve temporally the pulses from all photodiodes used. The RIN PSD is obtained by post-processing this signal following these steps: estimation of the sequence of pulse energies using a detection of the maximum of each pulse, normalization by the mean energy, and Fourier transform. These setups allow us to measure a RIN PSD and the corresponding IRINs from 250 Hz to 50 kHz for intraDFG and for DFG architectures.

3. Results and discussion

3.1. NIR to MIR noise transfer for DFG and intraDFG sources

We first measure the RIN of the pump at $1\ \mu\text{m}$ and of the output MIR beam at $8\ \mu\text{m}$ central wavelength to analyze the noise transfer process for both sources. These measurements are reported in Fig. 4.

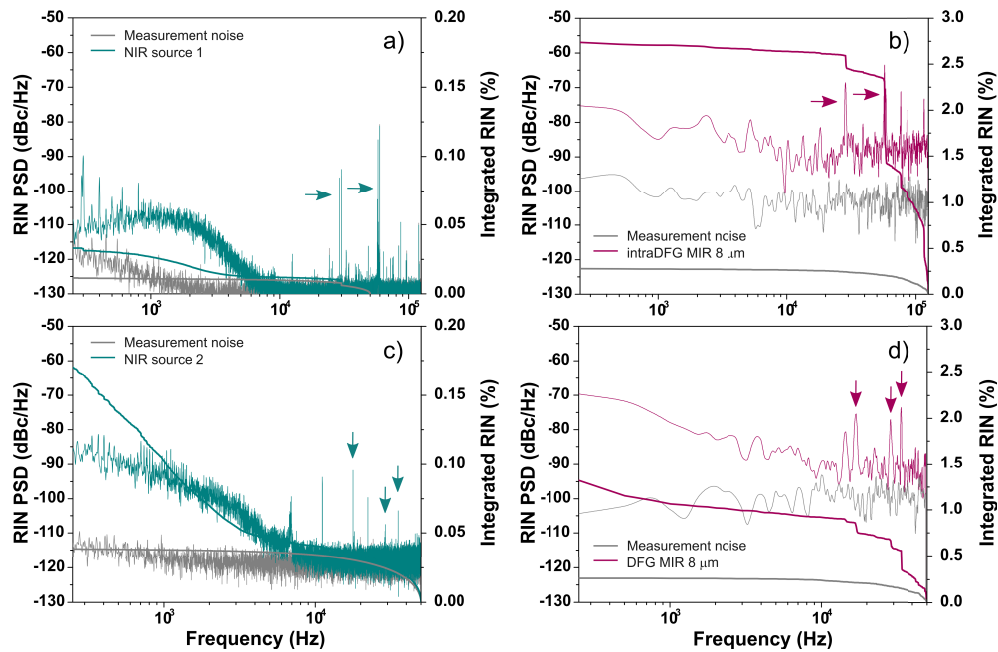


Fig. 4. Top: intraDFG RIN measurements of the (a) NIR pump driving source 1 before nonlinear compression (green) and (b) output MIR beam of source 1 with a spectrum corresponding to the red-filled curve in Fig. 2(a), shown over the frequency range [250 Hz - 125 kHz]. Bottom: DFG RIN measurements of the (c) NIR pump driving source 2 (green) and (d) output MIR beam of source 2 with a spectrum corresponding to the red solid line in Fig. 2(a), shown over the frequency range [250 Hz - 50 kHz]. In all cases, the measurement noise floors are shown in grey.

The IRIN of the NIR pump over the whole frequency span are 0.08% RMS and 0.34% RMS for sources 1 and 2 [1 Hz - 50 kHz], respectively. The corresponding measured pulse-to-pulse stabilities are 0.26% RMS and 0.35% RMS.

Let us first consider the RIN PSD in 4(a), corresponding to the pump of source 1. There is a quasi-white noise contribution for frequencies lower than 5 kHz. At higher frequencies the RIN

PSD goes down to the measurement floor, less than -125 dBc/Hz, but two peaks corresponding to technical noise contributions remain at 30 kHz and 60 kHz. The discrepancy between source 1 IRIN and pulse-to-pulse stability can be attributed to the fact that the electronic filter attenuates the peak at 60 kHz in the IRIN. The pulse-to-pulse noise measured in the MIR for source 1, based on intraDFG, is 3.5% RMS. The measured RIN in the MIR in this case is shown in Fig. 4(b). The IRIN over the whole frequency span is 2.7% RMS. This number shows that the relative intensity noise is increased through the DFG process. The noise peaks at 30 kHz and 60 kHz, observed in the NIR, are transferred and amplified in the MIR.

For source 2, in the NIR, a similar behavior at low frequency (<5 kHz) is observed for the RIN PSD plotted in Fig. 4(c). The impact of high frequency technical noise is less important in this case. Technical noise peaks at 11 kHz, 17 kHz, 28 kHz and 35 kHz are measured. The pulse-to-pulse noise measured in the MIR in this case is 1.4%, and the IRIN is 1.3% RMS, as shown in Fig. 4(d). As in the intraDFG case, the noise is amplified in the MIR and the technical noise peaks observed in the NIR RIN PSD are transferred and amplified in the MIR RIN PSD.

Upon inspection of Fig. 4(b) it is clear that the biggest noise contribution to the overall MIR noise in source 1 comes from technical noise of the pump amplified in the nonlinear intraDFG process. To reduce the intensity noise level in the MIR, we modify source 1 to remove the technical noise peaks at 30 kHz and 60 kHz observed in the NIR RIN PSD. This is done by synchronizing the RF wave driving the acousto-optic modulator used for pulse picking with the repetition rate of the laser, as demonstrated in [22]. After modification, the measured RIN in the MIR is shown in Fig. 5. It is flat over the whole measurement frequency range without any of the previously observed peaks.

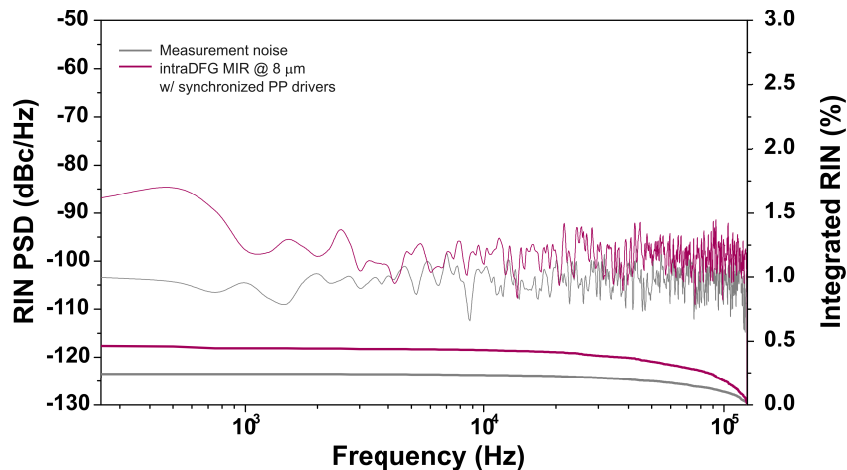


Fig. 5. MIR RIN measurement after source 1 modification.

The measured pulse-to-pulse stability in this case is 1% RMS. The IRIN is 0.4% RMS. Overall, this confirms that improving the driving source noise has a major effect on the MIR beam intensity noise performance, because of the nonlinear noise transfer process.

3.2. Intensity noise as a function of central wavelength for the intraDFG source

We now investigate how the intensity noise varies over the MIR tunability range, starting with the intraDFG source. We first analyze the intensity noise of different spectral parts of the nonlinearly compressed NIR driving source. References [23,24] report on the impact of intensity noise at the input of a SPM process: because of the intensity-dependent spectral broadening, there is an anti-correlated behavior between the central wavelength and the wings of the broadband

spectrum. On the contrary, the conjugated wavelength pairs on both sides of the SPM-broadened spectrum present strong correlations. This is clearly observed in the correlation measurement shown in Fig. 6(a), between the wavelength range $\lambda < 950$ nm and > 1100 nm of the few-cycle driving source, respectively filtered with shortpass (SP) and longpass (LP) filters.

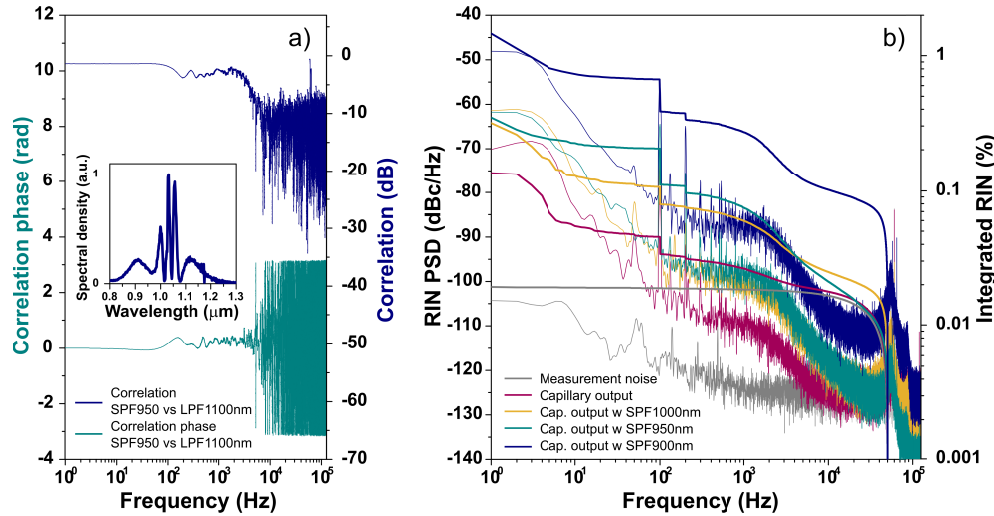


Fig. 6. (a) Correlation (amplitude and phase) of the short and long wavelength spectral parts of the compressed driving NIR pulse in source 1. Inset: broadened spectrum at the output of the capillary. (b) Relative intensity noise measurements without (red) and with shortpass filter at 1000 nm (yellow), 945 nm (green) and 900 nm (blue) at the output of the gas-filled capillary in source 1. The noise floor is in grey.

We now focus on the blue-side of the pump spectrum where silicon-based detectors can be used. In Fig. 6(b), the RIN measurements are reported for 4 different configurations where we have filtered part of the spectrum: (i) without optical filter, (ii) with SP filters presenting a cut-off wavelength of 1000 nm (FES1000, Thorlabs), (iii) 945 nm (945/SP BrightLine HC, Semrock), and (iv) 900 nm (FELH0900, Thorlabs). The IRIN are respectively 0.13, 0.32, 0.35 and 1.46% RMS over the frequency range [1 Hz - 50 kHz]. As expected, intensity noise levels increase while increasingly selecting the edge of the spectrum, because intensity-dependent spectral broadening results in fluctuations rejected to the edges of the broadened spectrum [23]. This leads to a global increase of the noise level over the whole NIR RIN PSD, as shown in Fig. 6(b).

We measure the intensity noise in the MIR while tuning the central wavelength from 8 to 4 μm . The measured RIN are reported in Fig. 7(a) and the corresponding pulse energies are plotted in Fig. 7(b). IRIN levels extend over a large range from 0.4 to 11% RMS, degrading from higher to lower wavelengths. Pulse-to-pulse stability measurements results, displayed in Fig. 7(b) confirm this behavior.

This observed MIR intensity noise behavior can be traced back to the intraDFG process: the pump and signal spectral parts enrolled in the nonlinear process to generate a short-wavelength idler (for instance, at $\lambda = 4\mu\text{m}$) are at the extreme wings of the NIR broadened spectrum, that fluctuate the most. In contrast, the long-wavelength idler (at $\lambda = 8\mu\text{m}$) is generated by mixing pump and signal closer to the central wavelength of the NIR spectrum at 1030 nm, spectral regions that exhibit less intensity fluctuations.

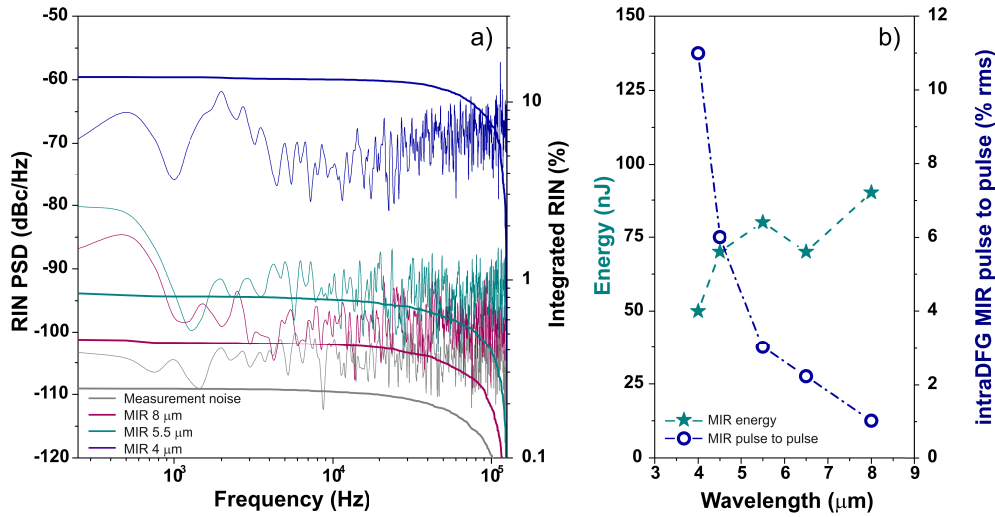


Fig. 7. (a) RIN measurements for the intraDFG source at 8 μm (red) 5.5 μm (green) and 4 μm (blue). (b) Pulse-to-pulse stability (blue) and pulse energy (green) as a function of MIR central wavelength.

3.3. Intensity noise as a function of central wavelength for the DFG source

The MIR intensity noise over the spectrum tunability of the DFG-based source 2 is now studied. We start with the noise analysis of the OPA delivering the signal for the DFG process.

As a preliminary step, the WLG stage is optimized to get the best possible pulse-to-pulse stability [25], before reaching the double filament regime. At the output of the YAG crystal we measure a stability of 0.75% RMS. The measured pulse-to-pulse stability of the DFG signal at the input of the LGS (output of the OPA) from 1150 nm to 1450 nm varies between 0.7 and 1.3%

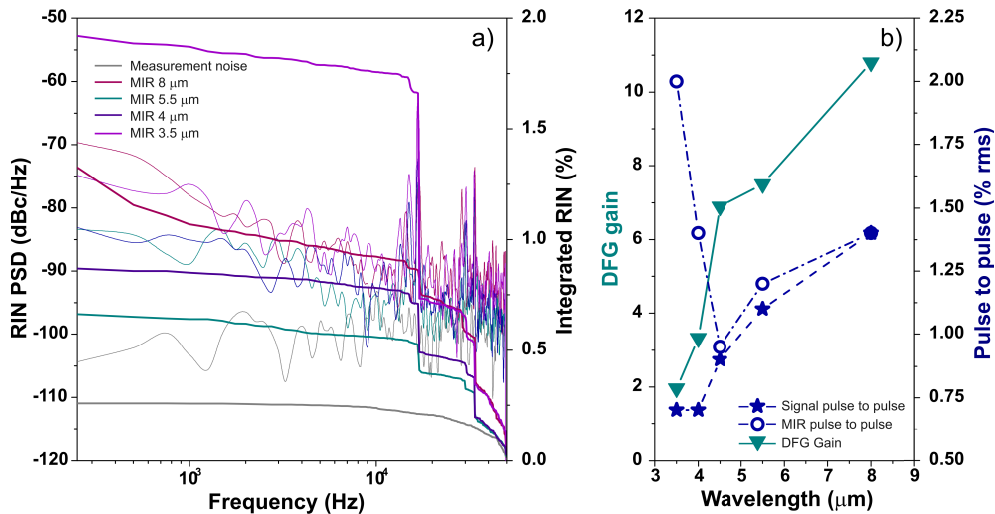


Fig. 8. (a) RIN measurements for the DFG source at 8 μm (red) 5.5 μm (green), 4 μm (blue), and 3.5 μm (violet). (b) Gain in the DFG crystal (green) and pulse-to-pulse stability of the seed at the input of the DFG (blue stars) and of the idler at the output of the DFG (blue circles).

RMS. This is most likely related to the properties of supercontinuum generation in the YAG crystal. Indeed this process is known to result in intensity fluctuations that depend on the spectral band considered [26,27]. We measure the RIN in the MIR while tuning the spectrum central wavelength from 8 μm down to 3.5 μm . Results are shown in Fig. 8(a). The IRIN varies from 0.6% RMS to 1.9% RMS going from higher to lower central wavelength. It should be noted that for source 2, the RF wave driving the acousto-optic modulator used for pulse picking has not been synchronized with the laser's repetition rate. This explains why peaks at 11 kHz, 17 kHz, 28 kHz, and 35 kHz are still present.

In order to understand these results, the MIR output and OPA signal pulse-to-pulse stabilities and the gain in the LGS crystal are plotted as a function of central MIR wavelength in Fig. 8(b). Two regions can be distinguished: from 8 to 4.5 μm MIR central wavelengths, a direct connection between OPA and MIR pulse-to-pulse stability is observed. In this region, where the gain in the LGS crystal is high enough, the signal intensity noise level appears to be the limiting factor for the MIR noise [28]. In the second region extending from 4.5 to 3.5 μm , this behavior disappears. Indeed, group velocity mismatch between pump and idler is higher for lower MIR wavelength therefore leading to a lower gain in the LGS crystal. This lower gain means that the amplification is not saturated, suppressing a noise reduction mechanism. The MIR intensity noise increases as the wavelength decreases and reaches its maximum at 3.5 μm , where a 1.9% RMS pulse-to-pulse stability is measured.

4. Conclusion

We have studied the intensity noise properties of tunable (from 3.5 to 11 μm) DFG-based MIR sources. Both an intraDFG setup pumped by a nonlinearly compressed ytterbium ultrafast source and a DFG architecture pumped by a similar ytterbium system are characterized.

First, we have measured the noise transfer from NIR Yb-doped laser to the MIR at 8 μm . For both realized setups the NIR noise is transferred and amplified in the MIR: it passes from <0.4% RMS in the NIR to 2.7% RMS and 1.4% RMS for the intraDFG and DFG case respectively. Significant improvement of the noise properties for the intraDFG source was shown by working to reduce the input NIR pump noise.

Second, we have measured and analyzed the intensity noise of these sources as a function of central wavelength over the octave-spanning tunability range. For the intraDFG source, the features of the noise dependence to central wavelength can be explained by the SPM process used to compress the driving pulses down to few-cycle durations, along with the fact that the spectral parts of the compressed pulses enrolled in the intraDFG interaction evolve as the source is tuned. As a result, the MIR source presents a pulse-to-pulse stability that decreases from 11 to 0.4% RMS when the wavelength increases. The delivered MIR energy level remains stable in the whole spectral range. For the DFG source, a pulse-to-pulse stability spanning from 0.6 to 1.9% RMS in the range 3.5-8 μm is measured. In this case an interplay between the pump-related gain and the signal intensity noise is observed, explaining the MIR noise level variations across the tuning spectrum.

These results bring a clearer understanding of the intensity noise properties and coupling in these laser sources based on nonlinear mixing of ultrafast pulses. This should help the design of low-noise high repetition rate sources in the MIR for applications such as time-resolved molecular spectroscopy. For example, if carrier-envelope phase stability is not required, the interpulse architecture RIN is less sensitive to the pump laser noise performance.

Funding. Agence Nationale de la Recherche (ANR-10-LABX-0039-PALM, ANR-19-CE30-0001-MIRTHYX).

Disclosures. The authors declare no conflicts of interest.

Data availability. Data underlying the results presented in this Letter are not publicly available at this time but may be obtained from the authors upon reasonable request.

References

1. M. Di Donato and M. L. Groot, "Ultrafast infrared spectroscopy in photosynthesis," *Biochimica et Biophys. Acta (BBA)-Bioenergetics* **1847**(1), 2–11 (2015).
2. J. P. Ogilvie and K. J. Kubarych, "Multidimensional electronic and vibrational spectroscopy: An ultrafast probe of molecular relaxation and reaction dynamics," *Adv. At., Mol., Opt. Phys.* **57**, 249–321 (2009).
3. J. Ye, L.-S. Ma, and J. L. Hall, "Ultrasensitive detections in atomic and molecular physics: demonstration in molecular overtone spectroscopy," *J. Opt. Soc. Am. B* **15**(1), 6–15 (1998).
4. A. Foltynowicz, T. Ban, P. Masłowski, F. Adler, and J. Ye, "Quantum-noise-limited optical frequency comb spectroscopy," *Phys. Rev. Lett.* **107**(23), 233002 (2011).
5. B. M. Luther, K. M. Tracy, M. Gerrity, S. Brown, and A. T. Krummel, "2D IR spectroscopy at 100 kHz utilizing a Mid-IR OPCPA laser source," *Opt. Express* **24**(4), 4117–4127 (2016).
6. H. Pires, M. Baudisch, D. Sanchez, M. Hemmer, and J. Biegert, "Ultrashort pulse generation in the Mid-IR," *Prog. Quantum Electron.* **43**, 1–30 (2015).
7. J. Ma, Z. Qin, G. Xie, L. Qian, and D. Tang, "Review of mid-infrared mode-locked laser sources in the 2.0 μm –3.5 μm spectral region," *Appl. Phys. Rev.* **6**(2), 021317 (2019).
8. A. Schliesser, N. Picqué, and T. W. Hänsch, "Mid-infrared frequency combs," *Nat. Photonics* **6**(7), 440–449 (2012).
9. Z. Heiner, V. Petrov, and M. Mero, "Efficient, sub-4-cycle, 1- μm -pumped optical parametric amplifier at 10 μm based on bga 4 s 7," *Opt. Lett.* **45**(20), 5692–5695 (2020).
10. M. Seidel, X. Xiao, S. A. Hussain, G. Arisholm, A. Hartung, K. T. Zawilski, P. G. Schunemann, F. Habel, M. Trubetskov, V. Pervak, O. Pronin, and F. Krausz, "Multi-watt, multi-octave, mid-infrared femtosecond source," *Sci. Adv.* **4**(4), eaaq1526 (2018).
11. R. Budriūnas, K. Jurkus, M. Vengris, and A. Varanavičius, "Long seed, short pump: converting yb-doped laser radiation to multi- μJ few-cycle pulses tunable through 2.5–15 μm ," *Opt. Express* **30**(8), 13009–13023 (2022).
12. I. Pupeza, D. Sánchez, J. Zhang, N. Lilienfein, M. Seidel, N. Karpowicz, T. Paasch-Colberg, I. Znakovskaya, M. Pescher, W. Schweinberger, V. Pervak, E. Fill, O. Pronin, Z. Wei, F. Krausz, A. Apolonski, and J. Biegert, "High-power sub-two-cycle mid-infrared pulses at 100 MHz repetition rate," *Nat. Photonics* **9**(11), 721–724 (2015).
13. A. Weigel, P. Jacob, D. Gröters, T. Buberl, M. Huber, M. Trubetskov, J. Heberle, and I. Pupeza, "Ultra-rapid electro-optic sampling of octave-spanning mid-infrared waveforms," *Opt. Express* **29**(13), 20747–20764 (2021).
14. T. Steinle, F. Mörz, A. Steinmann, and H. Giessen, "Ultra-stable high average power femtosecond laser system tunable from 1.33 to 20 μm ," *Opt. Lett.* **41**(21), 4863–4866 (2016).
15. M. Huber, W. Schweinberger, F. Stutzki, J. Limpert, I. Pupeza, and O. Pronin, "Active intensity noise suppression for a broadband mid-infrared laser source," *Opt. Express* **25**(19), 22499–22509 (2017).
16. P. Hamm, R. A. Kaindl, and J. Stenger, "Noise suppression in femtosecond mid-infrared light sources," *Opt. Lett.* **25**(24), 1798–1800 (2000).
17. W. Chen, J. Fan, A. Ge, H. Song, Y. Song, B. Liu, L. Chai, C. Wang, and M. Hu, "Intensity and temporal noise characteristics in femtosecond optical parametric amplifiers," *Opt. Express* **25**(25), 31263–31272 (2017).
18. Q. Bournet, F. Guichard, M. Natile, Y. Zaouter, M. Joffre, A. Bonvalet, I. Pupeza, C. Hofer, F. Druon, M. Hanna, and P. Georges, "Enhanced intrapulse difference frequency generation in the mid-infrared by a spectrally dependent polarization state," *Opt. Lett.* **47**(2), 261–264 (2022).
19. L. Lavenu, M. Natile, F. Guichard, X. Délen, M. Hanna, Y. Zaouter, and P. Georges, "High-power two-cycle ultrafast source based on hybrid nonlinear compression," *Opt. Express* **27**(3), 1958–1967 (2019).
20. K. Kato, K. Miyata, L. Isaenko, S. Lobanov, V. Vedenyapin, and V. Petrov, "Phase-matching properties of ligas 2 in the 1.025–10.5910 μm spectral range," *Opt. Lett.* **42**(21), 4363–4366 (2017).
21. Q. Bournet, M. Jonusas, A. Zheng, F. Guichard, M. Natile, Y. Zaouter, M. Joffre, A. Bonvalet, F. Druon, M. Hanna, and P. Georges, "Inline amplification of mid-infrared intrapulse difference frequency generation," *Opt. Lett.* **47**(19), 4885–4888 (2022).
22. O. De Vries, T. Saule, M. Plötner, F. Lücking, T. Eidam, A. Hoffmann, A. Klenke, S. Hädrich, J. Limpert, S. Holzberger, T. Schreiber, R. Eberhardt, I. Pupeza, and A. Tünnermann, "Acousto-optic pulse picking scheme with carrier-frequency-to-pulse-repetition-rate synchronization," *Opt. Express* **23**(15), 19586–19595 (2015).
23. P. Béjot, J. Kasparian, E. Salmon, R. Ackermann, N. Gisin, and J.-P. Wolf, "Laser noise reduction in air," *Appl. Phys. Lett.* **88**(25), 251112 (2006).
24. T. Godin, B. Wetzel, T. Sylvestre, L. Larger, A. Kudlinski, A. Mussot, A. B. Salem, M. Zghal, G. Genty, F. Dias, and J. M. Dudley, "Real time noise and wavelength correlations in octave-spanning supercontinuum generation," *Opt. Express* **21**(15), 18452–18460 (2013).
25. M. Natile, F. Guichard, Y. Zaouter, M. Hanna, and P. Georges, "Simple carrier-envelope phase control and stabilization scheme for difference frequency generation-based systems," *Opt. Express* **29**(11), 16261–16269 (2021).
26. M. Bradler and E. Riedle, "Temporal and spectral correlations in bulk continua and improved use in transient spectroscopy," *J. Opt. Soc. Am. B* **31**(7), 1465–1475 (2014).
27. D. Majus and A. Dubietis, "Statistical properties of ultrafast supercontinuum generated by femtosecond gaussian and bessel beams: a comparative study," *J. Opt. Soc. Am. B* **30**(4), 994–999 (2013).
28. L. Zhou, Y. Liu, G. Xie, C. Gu, Z. Deng, Z. Zhu, C. Ouyang, Z. Zuo, D. Luo, B. Wu, W. Li, and K. Chen, "Mid-infrared optical frequency comb in the 2.7–4.0 μm range via difference frequency generation from a compact laser system," *High Power Laser Sci. Eng.* **8**, e32 (2020).